THE FEASIBILITY OF Ni-ALUMINA CATALYSTS IN OXIDATIVE DEHYDROGENATION OF ETHANE

Libor ČAPEK[1,*], Lukáš VANĚK[2], Lucie SMOLÁKOVÁ[3], Roman BULÁNEK[4] and Jiří ADAM[5]

Department of Physical Chemistry, Faculty of Chemical Technology, University of Pardubice, Nám. Čs. Legií 565, 532 10 Pardubice, Czech Republic;
e-mail: [1] libor.capek@upce.cz, [2] vanek.lu@seznam.cz, [3] LucieSmolakova@seznam.cz, [4] roman.bulanek@upce.cz, [5] pavel.cicmanec@upce.cz

Received May 14, 2008
Accepted August 18, 2008
Published online October 3, 2008

The contribution deals with the development on the efficient Ni-alumina catalyst for the oxidative dehydrogenation (ODH) of ethane to ethene. The performance of Ni-alumina catalysts with varying nickel loadings and with thermal pretreatment was studied. We contribute to the understanding of the relationship between the activity of nickel species in ODH of ethane and its distribution. To analyze this effect, Ni-alumina catalysts were analyzed by UV-VIS spectroscopy, and H_2-TPR profile. Ni-alumina catalysts were highly active and selective (ca. 80%) in the ODH of ethane. The catalysts contained both tetrahedral and octahedral nickel species, suggesting that nickel aluminate represented a partial spinel, where Ni(II) ions occupy both octahedral and tetrahedral sites of the oxygen lattice. It was suggested that the octahedral nickel species were more active than the tetrahedral ones.
Keywords: Oxidative dehydrogenation; Ethane; Nickel; Alumina; UV-VIS; H_2-TPR.

Ethene is a very important industrial chemical. It is mainly used to produce ethylbenzene (styrene), vinyl chloride (polyvinyl chloride) and polyethylene (LDPE, HDPE and LLDPE). Steam cracking, fluid-catalytic cracking and catalytic dehydrogenation are currently used to produce ethene. However, these processes are thermodynamically limited. They also require high energy input due to their endothermic character and often catalyst regeneration due to coke formation. Thus, attention is currently focused to oxidative dehydrogenation (ODH) of ethane, which is assumed to be an alternative to classical processes of the ethene production. In ODH, the abstracted hydrogen is oxidized, releasing the reaction heat (exothermic process) and this activity becomes significant at lower temperature. ODH of ethane avoids the thermodynamic restrictions of non-oxidative routes by forming water as a by-product.

Collect. Czech. Chem. Commun. 2008, Vol. 73, Nos. 8–9, pp. 1177–1191

doi:10.1135/cccc20081177

A large number of catalysts have been studied in ODH of ethane. They encompass: (i) mixed oxide catalysts containing, for example, vanadium, molybdenum and niobium[1], and (ii) supported metal species, such as vanadium, on inorganic solids[2,3] or micro- and mesoporous materials[4]. In spite of intensive research, a low yield/selectivity of the reaction still prevent its industrial applications[5]. Cavani et al.[5] reported in the recent review that the most catalytic systems give the ethene yield below 20%. However, it should be mentioned, that there are many superior catalytic systems based on mixed oxides, such as Mo-V-Te-Nb-O [1], achieving the ethene yield above 40%.

The activity of Ni-based catalysts was reported with inconsistent results in ODH of ethane. Nakamura et al.[6] reported high activity of NiO-MgO, but negligible activity of Ni-alumina in ODH of ethane. Heracleous et al.[7] reported high activity of Ni-alumina in ODH of ethane starting already at 400 °C using W/F (the weight of catalyst to total flow rate) 0.54 g s ml^{-1}. Chang et al.[8] excluded Ni-ZSM-5 from being a good ODH catalyst due to an extremely high activity in generation of methane. Heracleous et al.[9] also reported high activity of Ni-Nb-O mixed oxide in the ethene production.

The present contribution deals with the development of an efficient Ni-alumina catalyst for the oxidative dehydrogenation (ODH) of ethane to ethene. In this work we attempt to contribute to understanding the activity of nickel-containing alumina catalysts in ODH of ethane. Ni-alumina catalysts were prepared with various nickel contents and various thermal pretreatment achieving different distributions of nickel species. To analyze the effect of nickel concentration on distribution of nickel species and their activity, Ni-based catalysts were characterized by UV-VIS spectroscopy and H_2-TPR profile.

EXPERIMENTAL

γ-Alumina (255 m^2 g^{-1}) was supplied by Eurosupport. Nickel-based catalysts (1.5, 2.9, 4.1 and 6 wt.% Ni) were prepared by impregnating alumina with a solution of nickel acetylacetonate in ethanol (as-prepared catalysts). After impregnation, the catalysts were filtered and dried for 24 h at room temperature. Finally, calcinations were performed in air at 600 (standard process) or 800 °C for 8 h.

UV-VIS diffuse reflectance spectra of dehydrated granulated (0.25–0.50 mm diamter) materials were recorded using GBS CINTRA 303 spectrometer equipped with a diffuse reflectance devise with a spectralon-coated integrating sphere against a spectralon reference. The reflectances were recalculated to absorption using the Schuster–Kubelka–Munk ($F(R_\infty)$) function, $F(R_\infty) = (1 - R_\infty)^2/2R_\infty$, in which R_∞ is the diffuse reflectance from a semi-infinite layer. The dehydration of nickel-based catalysts was carried out in the stream of oxygen in two steps: 120 °C for 30 min and 450 °C for 60 min. Thus the reactor was cooled down to 150 °C and evacuated for 30 min. After dehydration, the samples were cooled down to ambient

temperature and transferred into on optical cell of 5 mm thickness under vacuum and sealed.

The H_2-TPR (temperature-programmed reduction) profile was monitored with a heating rate 10 °C min^{-1} in the temperature range 20–900 °C. A Quartz microreactor was charged with 150 mg of a dry catalyst. Prior to the measurements, all the samples were activated at 450 °C for 2 h with a heating rate 10 °C min^{-1}. The reduction gas contained 5 vol.% H_2 in nitrogen with total flow rate 25 ml min^{-1}. A thermal conductivity detector monitored hydrogen consumption. The water produced by the sample reduction was frozen out in a cold trap using the mixture of ethanol and dry ice (at –76 °C) before input to the detector.

The oxidative dehydrogenation of ethane was carried out in a quartz through-flow micro-reactor at 500–700 °C and atmospheric pressure, typically with 200 mg of the catalyst (0.25–0.50 mm) diluted with 1 cm^3 of silicon carbide inert. The reaction mixture (considering of 9 vol.% C_2H_6, 2.5 vol.% O_2 and the rest was helium) was kept at a total flow of 100 ml min^{-1} (W/F 0.12 g_{cat} s ml^{-1}). The catalyst was activated in stream of oxygen at 450 °C for 1 h before the measurements. Gas chromatographic (Shimadzu) on-line analysis was carried out using Carboxen™ 1010 PLOT (30 m × 0.53 mm) and RT-S-PLOT (30 m × 0.53 mm) columns enabling separation and analysis of CO, CO_2, O_2, hydrocarbons, alcohols and aromatics.

RESULTS AND DISCUSSION

Characterization of Catalysts

Figure 1 shows the H_2-TPR profile of Ni-alumina catalysts. The intensive peak was observed at 797 °C. The peak maximum was shifted to a lower

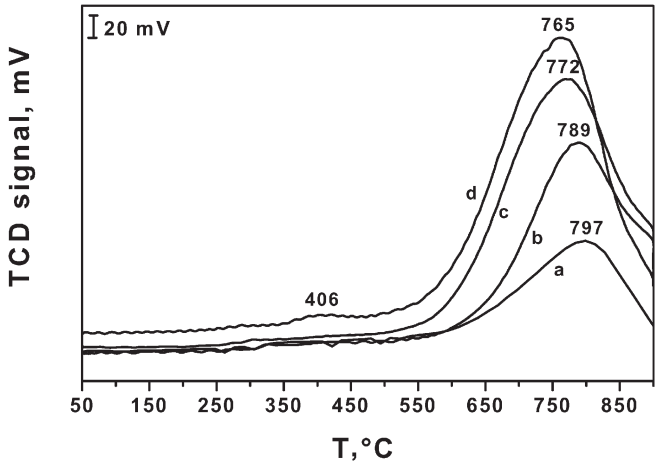

FIG. 1
H_2-TPR profile of Ni-alumina catalysts with 1.5 (a), 2.9 (b), 4.1 (c) and 6.0 (d) wt.% Ni

temperature with increasing nickel content. This peak could be attributed to the reduction of Ni(II) ions. Slagtern at al.[10] reported the reduction of Ni(II) species on alumina support at 771 °C. Rynkowski et al.[11] described the role of Ni-alumina calcination on the shift of the peak maximum. A new peak was observed in the H_2-TPR profile of Ni-alumina with 6 wt.% Ni at 406 °C. The TPR pattern of bulk NiO has been studied by Brown et al.[12]. They found one peak for reduction of bulk NiO at 418 °C under conditions very similar to our experiment (hydrogen concentration 5% and heating rate 10 °C min^{-1}). The reducibility of Ni on alumina is generally more difficult than that of bulk NiO or Ni on silica. Reduction of Ni(II) on silica has been observed at temperatures about 407 °C (ref.[13]). The reduction is detected above 627 °C (ref.[14]). The shift of reduction process to higher temperatures compared with bulk NiO or Ni-SiO_2 can be ascribed to strong interaction of Ni(II) ions with alumina. The reduction of NiO-alumina and the effect of the experimental conditions on catalytic properties of the reduced systems have been well documented[15–28]. The more laborious reduction of NiO on alumina supports compared with bulk and silica-supported NiO has been ascribed to metal oxide-support interactions[14,19]. Non-stoichiometric and stoichiometric nickel aluminate have been identified, in amounts and with structural characteristics depending on the preparation conditions[16,19]. Incorporation of Al(III) into NiO surface layers in impregnation has also been evidenced[20,28]. Most of the studies on γ-alumina-supported nickel oxide concerned high-surface-area supports and nickel loadings (from nickel nitrate) higher than 5 wt.%. In contrast, low-surface-area supports (α-alumina) and metal loadings below 5 wt.% have been much less addressed. Molina and Poncelet[29] detected in the TPR spectra of NiO supported on γ-alumina two peaks, the relative intensity of which was influenced by Ni loading and calcination temperature. Some indication supported the formation of a nickel aluminate spinel-type phase when the solid was calcined at 600 °C and above accounting for the high temperatures needed to reduce nickel oxide.

Figure 2 shows UV-VIS spectra of as-prepared Ni-alumina catalysts with 1.5, 2.9, 4.1 and 6 wt.% Ni. The six intensive bands were observed in the UV-VIS spectra with a maximum at ~13400, ~14600, ~23900, ~25400, ~33500 and ~47200 cm^{-1}. Bands at 33500 and 47200 cm^{-1} could be clearly attributed to Ni(II)-O charge transfer (CT) transition.

The intensity of the bands at ~13400, ~14600, ~23900 and ~25400 cm^{-1} increased with increasing Ni concentration. The maxima of the individual bands were slightly shifted to lower wavenumbers with increasing Ni

content. These UV-VIS bands were very similar to those of $[Ni(H_2O)_6]^{2+}$ (refs[30,31]). Six-coordinated octahedral nickel is characterized by the three spin allowed transitions: $^3A_{2g} \rightarrow {}^3T_{2g}$, $^3A_{2g} \rightarrow {}^3T_{1g}$ and $^3A_{2g} \rightarrow {}^3T_{1g}$ (P) with maxima at 7000–13000, 11000–20000 and 19000–27000 cm^{-1}, respectively[30,32,33]. Bands at ~13400 and ~14600 cm^{-1} were associated with spin-allowed transitions $^3A_{2g} \rightarrow {}^3T_{1g}$ of nickel ions with local octahedral symmetry, and bands at ~23900 and ~25400 cm^{-1} were associated with the spin-allowed transition $^3A_{2g} \rightarrow {}^3T_{1g}$ (P) which correspond to octahedral nickel coordinated with water $[Ni(H_2O)_6]^{2+}$ (ref.[31]). The transition $^3A_{2g} \rightarrow {}^3T_{2g}$ of octahedral nickel coordinated with water $[Ni(H_2O)_6]^{2+}$ is characterized by the UV-VIS band[30] at 8500 cm^{-1}. Nevertheless, this value is out of the measured range of wavenumbers.

A new intensive band appeared in the UV-VIS spectrum of Ni-alumina with 6 wt.% Ni at 33500 cm^{-1}. A low-intensity band at 33500 cm^{-1} was present in the UV-VIS spectra of alumina support and Ni-alumina catalysts with 1.5, 2.9 and 4.1 wt.% Ni. The intensity of the band was similar for alumina support and Ni-alumina catalysts. Thus, while low intensive band in the UV-VIS spectra of the Ni-alumina catalysts originated from alumina support, the intensive band in the UV-VIS spectrum of the Ni-alumina with 6 wt.% Ni was due to the nickel species[34]. This band could be attributed to a NiO species as also evidenced from the formation a new low-reductive peak at 406 °C in the H_2-TPR profile of Ni-alumina with 6 wt.% Ni.

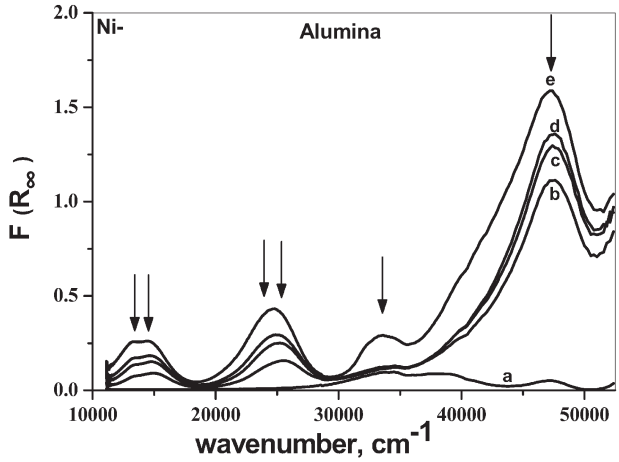

FIG. 2
UV-VIS spectra of as-prepared Ni-alumina catalysts with 0.0 (a), 1.5 (b), 2.9 (c), 4.1 (d) and 6.0 (e) wt.% Ni before its calcination

Figure 3 shows UV-VIS spectra of the dehydrated Ni-alumina catalysts with 1.5, 2.9, 4.1 and 6 wt.% Ni. The five intensive bands were observed in the UV-VIS spectra at ~15800, ~16900, ~24000, ~34700, ~40000 and ~47200 cm^{-1}. The calcinations led to the change in nickel species distribution. While the octahedral-nickel-coordinated species with water $[Ni(H_2O)_6]^{2+}$ were present in the Ni-alumina catalysts before their calcinations, the species were not present after its heat pretreatment, as evidenced by the absence of its characteristic UV-VIS bands at ~13400, ~14600, ~23900 and ~25400 cm^{-1}. The intensity of the individual bands increased with increasing Ni content from 1.5 to 4.1 wt.% Ni (1.5, 2.9 and 4.1 wt.% Ni). For Ni-alumina with 6 wt.% Ni, bands at ~15800 and ~16900 cm^{-1} increased in intensity, a new band appeared at ~27000 cm^{-1}, and bands at ~40000 and ~47200 cm^{-1} decreased in intensity.

Figure 4 shows the UV-VIS spectra of the dehydrated Ni-alumina catalyst with 2.9 wt.% Ni calcinated at 600 and 800 °C. The intensity of the UV-VIS bands at ~15800 and ~17000 cm^{-1} increased, but the intensity of the UV-VIS bands at ~24000 cm^{-1} and the bands above 30000 cm^{-1} decreased, if the calcinations were done at 800 °C instead of 600 °C. Thus, the UV-VIS bands at ~15800 and ~16900 cm^{-1} have to reflect the presence of a different nickel species in comparison with the UV-VIS band at ~24000 cm^{-1}.

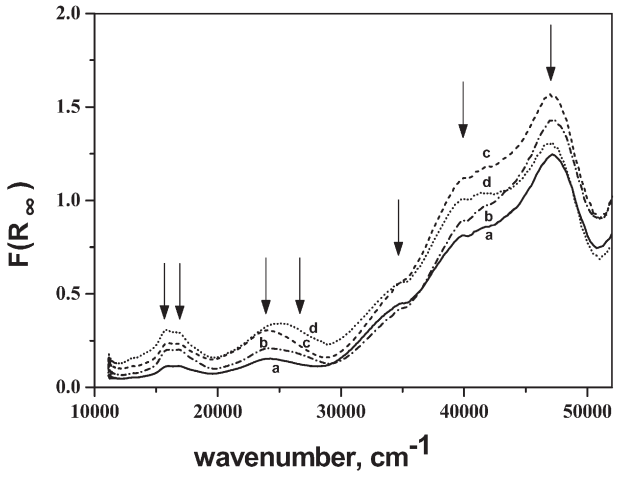

FIG. 3
UV-VIS spectra of dehydrated Ni-alumina catalysts with 1.5 (a), 2.9 (b), 4.1 (c) and 6.0 (d) wt.% Ni

The interaction between nickel and the alumina support is complex. Ni(II) can be dispersed on the alumina surface and also on the surface if nickel is incorporated into the spinel structure of alumina to form $NiAl_2O_4$. Moreover, nickel oxide (NiO) species could be weakly bounded on alumina support. Thus, it is very hard to distinguish between individual Ni species due to the complex catalyst structure.

The UV-VIS bands at ~15800 and ~16900 cm^{-1} (see Fig. 3) were attributed to the absorption bands of the tetrahedral Ni(II) in the alumina lattice, and not to octahedral Ni(II) species or NiO species (overlaps of characteristic bands are possible). This results from the observed shift in the UV-VIS bands at ~13400 and ~14600 cm^{-1} to ~15800 and ~16900 cm^{-1}, respectively, due to calcination procedure (Figs 2 and 3). Moreover, the UV-VIS bands at ~15800 and ~16900 cm^{-1} have to represent the presence of a different nickel species than that at ~24000 cm^{-1} (Fig. 4). The bands representing the nickel ions with local octahedral symmetry are present in the UV-VIS spectra at higher wavenumbers compared with the tetrahedral nickel species[31]. NiO species can be excluded from the Ni-alumina catalysts with 1.5, 2.9 and 4.1 wt.% Ni as it is evident from the absence of the sensitive low-reductive peak in the H_2-TPR profile at 406 °C (Fig. 1). In literature, the d-d electronic transition of the coordinated tetrahedral nickel ion species were reported to be present at ~14000 and ~15500 cm^{-1}, ~16700 and

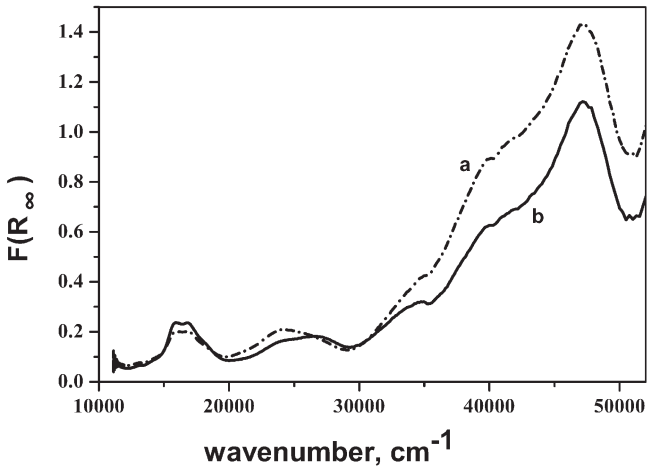

FIG. 4
UV-VIS spectra of dehydrated Ni-alumina catalyst with 2.9 wt.% Ni calcinated at 600 (a) and 800 (b) °C

~18000 cm^{-1}, which were attributed to the $^3T_1 \rightarrow {}^1E$, $^3T_1 \rightarrow {}^3T_1$ (P) and $^3T_1 \rightarrow {}^1T_2$, respectively[35–37]. Guevara-Lara et al.[31] reported the presence of the UV-VIS bands at 16051 and 15385 cm^{-1}, which they attributed to the spin-allowed transition $^3T_1 \rightarrow {}^3T_1$ (P) of nickel ions with local tetrahedral symmetry [$Ni^{2+}4O^{2-}$]. Heracleous et al.[7] reported the presence of the UV-VIS bands at 14000, 15600–16700 (doublet) and 18000 cm^{-1}, which they attributed to the $^3T_1 \rightarrow {}^1E$, $^3T_1 \rightarrow {}^3T_1$ (P) and $^3T_1 \rightarrow {}^1T_2$ transitions of tetrahedral Ni(II) ions in the alumina lattice. Jitianu et al.[38] identified absorption bands of tetrahedral Ni(II) ions in the alumina lattice at ~15500, ~16700 and ~18100 cm^{-1} and assigned them to the $^3T_1 \rightarrow {}^3T_1$ (P) and $^3T_1 \rightarrow {}^1T_2$ transitions, respectively.

On the other hand, the UV-VIS band at ~24000 cm^{-1} (see Fig. 3) was assigned to the d-d electronic transition of the octahedral Ni(II) ions in the alumina lattice[37,38], which was attributed to $^3A_{2g} \rightarrow {}^3T_{1g}$ (P) transition. Thus Ni-alumina catalysts prepared by impregnation of nickel acetylacetonate in ethanol led to the formation of both tetrahedral and octahedral nickel species in the alumina lattice.

The increase in the Ni content from 4.1 to 6 wt.% led to the formation of NiO species. This resulted in the formation of a new intensive band at ~27000 cm^{-1} in the UV-VIS spectrum of the dehydrated Ni-alumina catalyst with 6 wt.% Ni (Fig. 3), a new band at ~33500 cm^{-1} in the UV-VIS spectrum of the as-prepared Ni-alumina catalyst with 6 wt.% Ni (Fig. 2) and the formation of a new low-temperature reductive peak in the H_2-TPR profile at 406 °C (Fig. 1). Moreover, the formation of low-intensive bands at ~13000 and 14000 cm^{-1} was observed in the UV-VIS spectrum of Ni-alumina with 6 wt.% Ni (Fig. 3). The UV-VIS bands were similar to those of octahedral Ni(II) in NiO, which were reported to be characterized by the UV-VIS bands at ~26000, ~14000 and ~13000 cm^{-1}, representing the $^3A_{2g} \rightarrow {}^3T_{2g}$, $^3A_{2g} \rightarrow {}^3T_{1g}$ and $^3A_{2g} \rightarrow {}^3T_{1g}$ (P) transitions, respectively[38]. Li et al.[34] reported the characteristic UV-VIS band of NiO aggregates at ca. 25300 nm.

Activity of Ni-Alumina Catalysts in Oxidative Dehydrogenation of Ethane

Oxidative dehydrogenation (ODH) of ethane over nickel-based catalysts led predominantly to ethene, CO, and CO_2. CH_4 was formed starting from a trace concentration up to the 3% selectivity to methane, depending on the reaction conditions and Ni content. The formation of other hydrocarbons or its derivatives was not observed. The contribution of homogeneous gas-phase reactions was not observed in the whole range of reaction conditions

as resulted from the zero conversion of ethane and oxygen in a reactor without catalyst.

Figure 5 shows the dependence of the activity (ethane conversion, oxygen conversion, ethene yield and selectivity to ethene) on the reaction temperature in ODH of ethane over Ni-alumina with 4.1 wt.% Ni. The ethane conversion and ethene yield increased with increasing temperature. Selectivity to ethene was high in the whole temperature range. It was still keeping at around 80%. The rest was CO and CO_2 that formed in approximately same amounts. The oxygen conversion increased with increasing temperature and the ~100% value was achieved at 650 °C.

Data in Table II show the important role of oxygen in the activity of Ni-alumina catalyst. While Ni-alumina with 2.9 wt.% Ni was highly active and selective (X = 19.8%, S = 78.8%) in the ethene formation under oxygen presence, the same catalyst showed a very low activity in the oxygen absence (X = 5.5%, S = 92.6%). The activity of Ni-alumina catalyst was stable in ODH of ethane to ethene in the oxygen presence for 6 h time-on-stream. The oxygen presence is thus necessary for high ethene production.

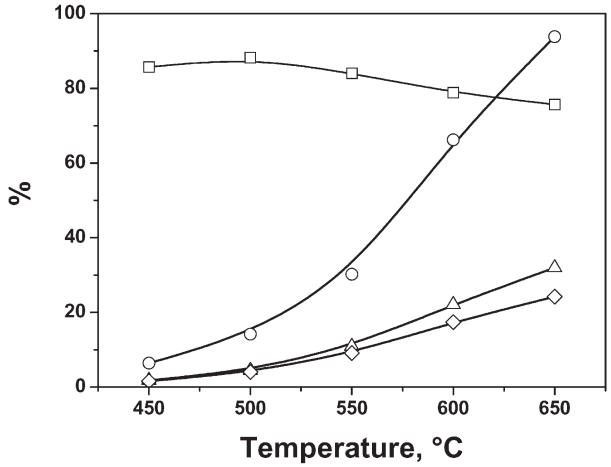

FIG. 5

Dependence of ethane conversion (△), ethene yield (◇), selectivity to ethene (□) and oxygen conversion (○) on temperature in ODH of ethane over Ni-alumina catalyst with 4.1 wt.% of Ni. Gas composition 9.0% ethane, 2.5% O_2 and He, 200 mg catalysts, total flow 100 ml min^{-1} and W/F 0.12 g_{cat} s ml^{-1}

Figure 6 shows the dependence of the activity (ethane conversion, oxygen conversion, ethene yield and selectivity to ethene) on the nickel content in the ODH of ethane at 550 °C (Fig. 6A), 600 °C (Fig. 6B) and 650 °C (Fig. 6C). At 550 °C, the ethane conversion and the ethene yield increased with increasing amount of nickel up to the maxim nickel content. On the other hand, at 600 and 650 °C the ethane concentration and ethene yield increased with increasing nickel content achieving a maximum value between 2.9 and 4.1 wt.% Ni. Then, the activity slightly decreased for the Ni-alumina with 6 wt.% Ni. An ethene yield of 9.6% was achieved at 550 °C (X = 11.2%, S = 85.2%), 16.4% at 600 °C (X = 21.1%, S = 79.3%) and 23.7% at 650 °C (X = 31.3%, S = 75.9%). The selectivity to CH_4 increased with increasing temperature. The selectivities to undesired CH_4 <0.5% at 550 °C, ~1% at 600 °C and ~3% at 650 °C were observed.

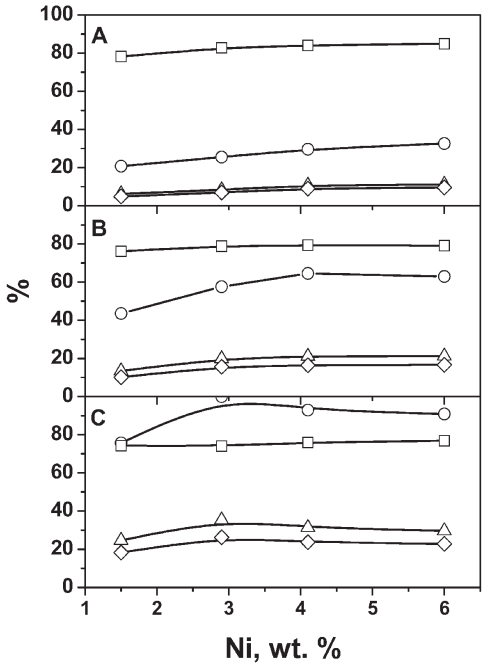

FIG. 6

Dependence of ethane conversion (△), ethene yield (◇), selectivity to ethene (□) and oxygen conversion (○) on nickel content in ODH of ethane over Ni-alumina catalysts at 550 (A), 600 (B) and 650 (C) °C. Gas composition 9.0% ethane, 2.5% O_2 and He, 550–650 °C, 200 mg catalysts, total flow 100 ml min^{-1} and W/F 0.12 g_{cat} s ml^{-1}

On addition to the ethene yield and the selectivity to ethene, the ethene productivity is an important property in ODH of ethane. The application of ODH of ethane requires at least the ethene productivity[5] 1 $g(C_2^=)\ g_{cat}^{-1}\ h^{-1}$. Table I contains the ethene productivity in ODH of ethane over Ni-alumina catalysts at 550, 600 and 650 °C. At 550 °C, it increased up to 0.29 $g(C_2^=)\ g_{cat}^{-1}\ h^{-1}$ with increasing Ni content. On the other hand, at 600 and 650 °C, the ethene productivity was similar for Ni-alumina catalysts with the Ni content between 2.9 and 6 wt.%. The ethene productivities 0.53 $g(C_2^=)\ g_{cat}^{-1}\ h^{-1}$ at 600 °C and 0.74 $g(C_2^=)\ g_{cat}^{-1}\ h^{-1}$ at 650 °C were observed. Most of the catalytic systems active in ODH of ethane has the ethene productivity below 0.35 $g(C_2^=)\ g_{cat}^{-1}\ h^{-1}$. For example, a high productivity was reported for V_2O_5-Al_2O_3 (0.24–0.79 $g(C_2^=)\ g_{cat}^{-1}\ h^{-1}$)[2,5],

TABLE I
Productivity of ethene in ODH of ethane over Ni-alumina catalysts. Gas composition 9.0% ethane, 2.5% O_2 and He, 550, 600 and 650 °C, 200 mg catalyst, total flow 100 ml min^{-1} and W/F 0.12 g_{cat} s ml^{-1}

Catalyst	Ni wt.%	Productivity, $g(C_2^=)\ g_{cat}^{-1}\ h^{-1}$		
		T = 550 °C	T = 600 °C	T = 650 °C
Ni-alumina	1.5	0.15	0.33	0.56
Ni-alumina	2.9	0.21	0.48	0.71
Ni-alumina	4.1	0.28	0.53	0.74
Ni-alumina	6.0	0.29	0.52	0.70

TABLE II
Transformation of ethane to ethene under oxygen presence and absence. Gas composition 9.0% ethane, 2.5% O_2 or 0.0% O_2 and He, 600 °C, 200 mg Ni-alumina catalyst with 2.9 wt.% Ni, total flow 100 ml min^{-1} and W/F 0.12 g_{cat} s ml^{-1}

Test	Ethane conversion, %	Selectivity to ethane, %	Ethene yield, %
Oxygen presence (ethane – O_2 – He)	19.8	78.8	15.6
Oxygen absence (ethane – He)	5.5	92.6	5.1

V-MCM-41 (0.14–0.76 $g(C_2^=)\ g_{cat}^{-1}\ h^{-1}$)[4,5] and mixed oxides containing alkali or alkaline earth metal oxides (above 1 $g(C_2^=)\ g_{cat}^{-1}\ h^{-1}$)[5,39]. It should be mentioned that the productivity reported for NiO-MgO catalyst was 6.35 $g(C_2^=)\ g_{cat}^{-1}\ h^{-1}$)[6]. But, the productivity reported for Ni-alumina catalysts were below 0.2 $g(C_2^=)\ g_{cat}^{-1}\ h^{-1}$ (refs[5–7]), even of those with giving high ethene yields. Thus the ethene productivity of Ni-alumina catalysts (Table I) was over average value; moreover, this was achieved at high ethene yields and selectivities. Heracleous et al.[7] observed a high catalytic activity of Ni-alumina at 400 °C (a very interesting temperature from the application viewpoint), which is a lower temperature than that shown here (Tables II and III, Fig. 5). The activity at a lower reaction temperature (400 °C) was reported at lower contact time (W/F 0.53 $g(C_2^=)\ g_{cat}^{-1}\ h^{-1}$)[7] compared with that used in this work (W/F 0.12 $g(C_2^=)\ g_{cat}^{-1}\ h^{-1}$). But, the ethene productivity (ca. 0.52 $g(C_2^=)\ g_{cat}^{-1}\ h^{-1}$ at 600 °C; Table I) was higher that that at 400 °C reported by Heracleous et al.[7] (ca. 0.2 $g(C_2^=)\ g_{cat}^{-1}\ h^{-1}$).

Data in Table III show the activity of Ni-alumina with 2.9 wt.% Ni calcined at 600 and 800 °C. It is clearly seen that the ethane conversion and the selectivity to ethene decreased due to its calcinations at higher temperature, i.e. at 800 °C. This is in contrast to the behavior of transition zeolite-based catalysts[40]. Nowinska et al.[40] reported that Fe-, Mn- and Co-ZSM-5 catalysts are active in ODH of propane if pretreated at 900 °C.

TABLE III

Dependence of the activity on temperature in ODH of ethane over Ni-alumina catalyst with 2.9 wt.% of Ni prepared by calcinations at 600 and 800 °C. Gas composition 9.0% ethane, 2.5% O_2 and He, 200 mg catalysts, total flow 100 mlTmin^{-1} and W/F 0.12 g_{cat} s ml^{-1}

Reaction temperature, °C	Calc. temperature, °C	Ethane conversion, %	Selectivity to ethane, %
550	600	8.1	83.4
	800	5.2	80.7
600	600	19.8	79.6
	800	11.6	77.1
650	600	30.6	75.9
	800	20.7	76.2

It was shown that both tetrahedral and octahedral nickel species in the alumina lattice were present in Ni-alumina catalysts (Fig. 3). Thus, it can be suggested that nickel aluminate is a partial spinel, which means Ni(II) ions occupy both octahedral and tetrahedral sites of the oxygen lattice[7]. Several authors postulated the existance of a "surface spinel" on the interface of Ni-alumina[41]. Lo Jacono et al.[41] proposed that this "surface spinel" accommodates octahedral and tetrahedral nickel sites.

The activity of Ni-alumina catalyst calcined at 800 °C was lower compared with that calcined at 600 °C (Table III). The calcinations at 800 °C led to a decrease in the intensity of the UV-VIS bands at ~24000 cm^{-1} reflecting the presence of the octahedral coordinated nickel species, and to an increase in the intensity of the UV-VIS bands at ~15800 and ~17000 cm^{-1} reflecting the presence of the tetrahedral-coordinated nickel species (Fig. 4). Thus, the Ni-alumina catalyst pretreated at 800 °C had a lower relative population of the octahedral nickel species. This is in agreement with the results of Wu at el.[42], who reported that the tetrahedrally coordinated nickel ions are difficult to reduce, whereas the octahedral nickel ions are readily reduced. On the other hand, Altamirano et al.[37] reported that calcinations of Co(Ni)MoS_2 catalysts at higher temperatures led to the formation of octahedral-coordinated instead of tetrahedral-coordinated nickel species.

Heracleous et al.[7] reported that both nickel aluminate-like species and NiO particles are active and selective in ODH of ethane. This contribution was focused in more detail on Ni-alumina catalysts not including NiO species. NiO species was not observed in Ni-alumina catalysts with 1.5, 2.9 and 4.1 wt.% Ni as clearly evidenced by the H_2-TPR profile (absence of low-temperature peak at 406 °C; Fig. 1). The results reported here specify the efficiency of nickel aluminate-like species in Ni-alumina with lower nickel contents. It can be suggested that octahedral nickel species were more effective than the tetrahedral ones. It was evidenced from a lower activity of the Ni-alumina catalyst with 2.9 wt.% Ni pretreated at 800 °C than that pretreated at 600 °C (Fig. 4, Table III).

CONCLUSIONS

The contribution deals with the catalytic performance of Ni-alumina catalysts with different nickel loadings in oxidative dehydrogenation (ODH) of ethane. The performance of Ni-alumina catalysts with varying nickel loadings and with varying temperature pretreatment was studied.

Ni-alumina was a highly active and selective catalyst in ODH of ethane. The highest activity was observed with the catalysts containing 2.9–4.1 wt.% Ni.

An interesting activity was observed at 600 °C (ethane conversion 21.1%, ethene yield 16.4%, selectivity to ethene 79.3%, ethene productivity 0.53 $g(C_2^=)\ g_{cat}^{-1}\ h^{-1}$) and 650 °C (31.3, 23.7 and 75.9%, ethene productivity 0.74 $g(C_2^=)\ g_{cat}^{-1}\ h^{-1}$, respectively). The selectivity to ethene was still keeping at around ~80% in a wide range of reaction temperatures and nickel contents. The ethene productivity represented for Ni-alumina catalysts was over the average values, which, moreover, was achieved at high ethene yields and selectivities.

The catalysts contained both tetrahedral and octahedral nickel species, suggesting that nickel aluminate represented a partial spinel structure, where Ni(II) ions occupy both octahedral and tetrahedral sites of the oxygen lattice. The decrease in Ni-alumina activity corresponded to the decrease in a relative population of the octahedral nickel species and to an increase in relative population of the tetrahedral nickel species. It was suggested that the former species were more effective than the letter.

The authors gratefully thank the Czech Science Foundation for financial support (projects No. 104/07/P038 and No. 203/08/H032) and the Ministry of Education, Youth and Sports of the Czech Republic (No. MSM0021627501).

REFERENCES

1. López-Nieto J. M., Botella P., Vázquez M. I., Dejoz A.: *Chem. Commun.* **2002**, 1906.
2. Martinez-Huerta M. V., Gao X., Tian H., Wachs I. E., Fierro J. L. G., Banares M. A.: *Catal. Today* **2006**, *118*, 279.
3. Solsana B., Dejoz A., Garcia A., Concepción P., López Nieto J. M., Vázquez M. I., Navarro M. T.: *Catal. Today* **2006**, *117*, 228.
4. Solsona B., Blasco T., López Nieto J. M., Peňa M. L., Rey F., Vidal-Moya A.: *J. Catal.* **2001**, *203*, 443.
5. Cavani F., Ballarini N., Cericola A.: *Catal. Today* **2007**, *127*, 113.
6. Nakamura K. I., Miyake T., Konishi T., Suzuki T.: *J. Mol. Catal. A* **2006**, *260*, 144.
7. Heracleous E., Lee A. F., Wilson K., Lemonidou A. A.: *J. Catal.* **2005**, *231*, 159.
8. Chang Y. F., Somorjai G. A., Heinemann H.: *Appl. Catal., A* **1993**, *96*, 305.
9. Heracleous E., Lemonidou A. A.: *J. Catal.* **2006**, *237*, 162.
10. Slagtern Å., Swaan H. M., Olsbye U., Dahl I. M., Mirodatos C.: *Catal. Today* **1998**, *46*, 107.
11. Rynkowski J. M., Paryjczak T., Lenik M.: *Appl. Catal., A* **1993**, *106*, 73.
12. Brown R., Cooper M. E., Whan D. A.: *Appl. Catal.* **1982**, *3*, 177.
13. Robertson S. D., McNicol B. D., de Baas J. H., Kloet S. C., Jenkins J. W.: *J. Catal.* **1975**, *37*, 424.
14. Parysczak T., Rynkowski J., Krzyzanowski V.: *React. Kinet. Catal. Lett.* **1982**, *21*, 295.
15. Bartholomew C. H., Pannell R. B., Fowler R. W.: *J. Catal.* **1983**, *79*, 34.
16. Hu J., Schwarz J. A.: *Appl. Catal.* **1989**, *51*, 223.

17. Rynkowski J. M., Paryjczal T., Lenik M.: *Appl. Catal., A* **1993**, *106*, 73.
18. Turlier P., Praliaud H., Moral P., Martin G. A., Dalmon J. A.: *Appl. Catal.* **1985**, *19*, 287.
19. Zielinski J.: *J. Catal.* **1982**, *76*, 157.
20. Richardson J. T., Lei M., Turk B., Forster K., Twigg M. V.: *Appl. Catal., A* **1994**, *110*, 217.
21. Reinen D., Selwood P. W.: *J. Catal.* **1963**, *2*, 109.
22. Bartholomew C. D., Ferrauto R. J.: *J. Catal.* **1976**, *45*, 41.
23. Bartholomew C. D., Pannell R. B.: *J. Catal.* **1980**, *65*, 390.
24. Vedrine J. C., Hollinger G., Duc T. M.: *J. Phys. Chem.* **1978**, *82*, 1515.
25. Houalla M., Lemaitre J., Delmon B.: *J. Chem. Soc., Faraday Trans.* **1982**, *78*, 1389.
26. Gavalas G. R., Phichitkul C., Voecks G. E.: *J. Catal.* **1984**, *88*, 54.
27. Gandia L. M., Montes M.: *J. Mol. Catal.* **1994**, *94*, 347.
28. Chen S. L., Zhang H. L., Hu J., Contescu C., Schwarz J. A.: *Appl. Catal.* **1991**, *73*, 289.
29. Molina R., Poncelet G.: *J. Catal.* **1998**, *173*, 257.
30. Lever A. B. P.: *Inorganic Elektronic Spectroscopy*, 2nd ed. Elsevier, Amsterdam 1984.
31. Guevara-Lara A., Bacaud R., Vrinat M.: *Appl. Catal., A* **2007**, *328*, 99.
32. Galoisy L., Calas G.: *Am. Mineral* **1991**, *76*, 1777.
33. Rossman G. R., Shannon R. D., Waring R. K.: *J. Solid. State Chem.* **1981**, *39*, 277.
34. Li D., Nishijima A., Morris D. E., Guthrie G. D.: *J. Catal.* **1999**, *188*, 111.
35. Cimino A., Jacono M. L., Schiavello M.: *J. Phys. Chem.* **1975**, *79*, 243.
36. Jacono M. L., Schiavelo M., de Beer V. H. J., Minelli G.: *J. Phys. Chem.* **1977**, *81*, 6.
37. Altamirano E., de los Reyes J. A., Murrieta F., Vrinat M.: *Catal. Today* **2008**, *133*, 292.
38. Jitianu M., Jitianu A., Zaharescu M., Crisan D., Marchidan R.: *Vib. Spectrosc.* **2000**, *22*, 75.
39. Dai H. X., Ng C. F., Au C. T.: *J. Catal.* **2001**, *197*, 251.
40. Nowinska K., Waclaw A., Izbinska A.: *Appl. Catal., A* **2003**, *243*, 225
41. Lojacono M., Schiavel M., Cimino A.: *J. Phys. Chem.* **1971**, *75*, 1044.
42. Wu M., Hercules D. M.: *J. Phys. Chem.* **1979**, *83*, 2003.